Appl Phys B (2012) 106:473–482
DOI 10.1007/s00340-011-4713-y

Applied Physics B
Lasers and Optics

Potential interference mechanism for the detection of explosives via laser-based standoff techniques

B. Wen · H. Eilers

Received: 8 April 2011 / Revised version: 11 July 2011 / Published online: 10 September 2011

Abstract A variety of laser-based standoff techniques are currently being developed for the detection of explosives. Many approaches focus on the detection of NO as an indicator for the presence of nitro-based explosives. One of these approaches uses lasers to vaporize the explosive molecules residing at or near a surface, photo-dissociate the molecules resulting in vibrationally hot NO, and then perform laser-induced fluorescence on the vibrationally hot NO. Most related reports have focused on using 236 nm or 247–248 nm for the laser excitation of vibrationally hot NO. In addition, a recent report suggests the use of 532 nm to desorb, vaporize, and photo-fragment explosive samples. We report here on energy transfer from laser-excited N_2 to NO and its consequences for the detection of nitro-based explosives. A potential interference mechanism was found for using 532 nm and 236 nm. The interference mechanism is based upon multi-photon excitation (532 nm) or two-photon excitation (236 nm) into excited states of molecular nitrogen and subsequent energy transfer from nitrogen to NO, followed by NO luminescence. Such interference mechanisms highlight the complexity of the explosive detection problem and the need for complementary approaches to improve the detection capabilities.

1 Introduction

The detection of explosives is a long-standing problem, and detection approaches and related problems have been widely described in the scientific literature [1–3]. With the events of 9/11, the subsequent military engagements in Afghanistan and Iraq, and various terrorists events and attempts during the last decade, the interest in improved explosion detection capabilities has increased significantly. Various bulk and trace detection system have been developed. However, for trace detection the low vapor pressure (ppbV level at room temperature) of many explosive compounds together with deliberate concealment makes detection very difficult [3]. Adding further difficulty, the detection approach becomes extremely complex when the process is to be applied in a dirty environment where unexploded ordnance and residues from explosions can contaminate the area. The need to detect explosives from a safe standoff distance adds another level of difficulty to developing useful detection approaches and techniques.

Many laser-based spectroscopy techniques have been characterized for standoff detection of explosives. Infrared [4, 5] and Raman [6–8] spectroscopy are based on detecting vibrational signatures of molecules. These techniques can result in some unique explosive signatures. However, because of the low cross sections for the underlying processes, they usually cannot detect low concentrations. The detection limits can be enhanced by variations such as cavity enhanced ring down spectroscopy or surface-enhanced Raman spectroscopy. Also, a UV gated Raman spectroscopy approach was recently reported to have two-orders-of-magnitude higher signals than visible light [9]. Improved signal quality was also reported for backward coherent anti-Stokes Raman scattering (B-CARS) [10]. However, many of these approaches are not suitable for standoff detection.

Various ultraviolet (UV) and visible light approaches have also been developed [11, 12]. While the cross-sections for absorption and fluorescence are higher than those for

B. Wen · H. Eilers (✉)
Institute for Shock Physics, Applied Sciences Laboratory,
Washington State University, Spokane, WA 99210-1495, USA
e-mail: eilers@wsu.edu
Fax: +1-509-3587728

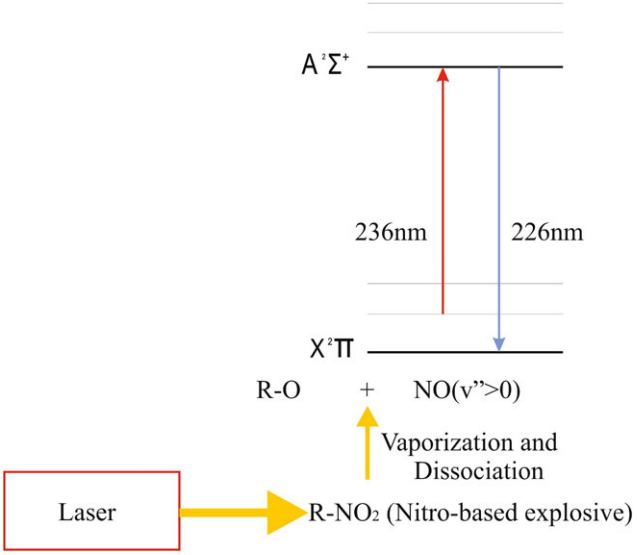

Fig. 1 Single-laser pulse based detection approach

vibrational spectroscopy, the spectral features are usually broad and featureless, providing no specific information on which molecules absorbed or emitted the light. An infrared CO_2 laser was recently used to heat explosive samples while the increased blackbody radiation was observed to monitor the temperature increase in the sample [13]. The authors were able to measure a signal at distances up to 150 m. However, no information of the amount of sample was given, beyond describing it as "trace."

Also, many fragmentation-based detection approaches have been developed. Explosive molecules are decomposed by thermal or laser-induced means and generate small gas molecules [3]. These molecules are then detected by various detection techniques, including laser-induced breakdown spectroscopy [14–18]. Many fragmentation approaches for the detection of nitro-based explosives focus on the detection of NO as an indicator for the presence of an explosive material. One of these approaches uses a laser to vaporize and photo-dissociate the explosive material molecules near the surface, resulting in vibrationally hot NO molecules, which are then detected via laser-induced fluorescence (LIF) [19–24]. Shu et al. focused on using a 248 nm laser to excite the $X^2\Pi$ $(v'' = 2) \rightarrow A^2\Sigma$ $(v' = 0)$ transition and observe the $A^2\Sigma$ $(v' = 0) \rightarrow X^2\Pi$ $(v'' = 0)$ fluorescence [19–21].

Arusi-Parpar et al. used 248 nm for the photodissociation followed by laser-induced fluorescence (LIF) at atmospheric pressure to detect 2,4,6-trinitrotoluene (TNT) vapor [25]. In their experiment, a single laser beam was used to induce the photodissociation of TNT vapor, followed by highly selective detection of its photofragments of vibrationally excited NO, and utilizing laser induced fluorescence with the $A^2\Sigma^+$ $(v' = 0) \leftarrow X^2\Pi$ $(v'' = 2)$ transition. Wynn et al. characterized and evaluated four different excitation schemes for the LIF of vibrationally hot NO: 1. Exc. $X^2\Pi$ $(v'' = 1) \rightarrow A^2\Sigma$ $(v' = 0)$ and flu. $A^2\Sigma$ $(v' = 0) \rightarrow X^2\Pi$ $(v'' = 0)$; 2. Exc. $X^2\Pi$ $(v'' = 1) \rightarrow A^2\Sigma$ $(v' = 1)$ and flu. $A^2\Sigma$ $(v' = 1) \rightarrow X^2\Pi$ $(v'' = 0)$; 3. Exc. $X^2\Pi$ $(v'' = 2) \rightarrow A^2\Sigma$ $(v' = 0)$ and flu. $A^2\Sigma$ $(v' = 0) \rightarrow X^2\Pi$ $(v'' = 0)$, and $A^2\Sigma$ $(v' = 0) \rightarrow X^2\Pi$ $(v'' = 1)$; and 4. Exc. $X^2\Pi$ $(v'' = 3) \rightarrow A^2\Sigma$ $(v' = 1)$ and flu. $A^2\Sigma$ $(v' = 1) \rightarrow X^2\Pi$ $(v'' = 1)$, and $A^2\Sigma$ $(v' = 1) \rightarrow X^2\Pi$ $(v'' = 0)$ [24].

All of these approaches are applied to solid samples and the advantage is that a single laser pulse can be used to perform the three steps of vaporizing the material, inducing the photo-dissociation, and exciting the vibrationally hot NO molecules, see Fig. 1. More recently, White et al. reported a slightly different approach. They used two lasers, a powerful 532 nm laser to desorb, vaporize, and photo-fragment the samples, and a second laser to stimulate the laser-induced fluorescence [22]. The advantage of this approach is that a much more powerful laser can be used to desorb, vaporize, and photo-fragment the samples.

While the above outlined approaches appear to be promising under certain conditions, it is not clear if and how atmospheric conditions, such as the presence of nitrogen and oxygen might affect these approaches. Shu et al. pointed out that NO is quenched by O_2 with a rate constant of 1.4×10^{-10} cm^3 s^{-1}, and by N_2 with a rate constant about three orders of magnitude lower [19]. However, other potential interference sources need to be considered for their effects on the laser-based detection of explosives. For example, it has been shown that molecular nitrogen can be excited by certain laser wavelengths through multi-photon processes [26, 27]. In addition, it is well-known that excited molecular nitrogen can transfer energy to NO [28–32]. As such, it is conceivable that laser-based detection approaches might suffer interferences from processes that are based on energy transfer from laser-excited species.

We report here on energy transfer from laser-excited nitrogen molecules to NO molecules for 532 nm and 236 nm excitation of NO/N_2 and NO/air mixtures, resulting in fluorescence at 226 nm from NO molecules without having vibrationally hot NO molecules present.

2 Experimental

The experimental setup is shown in Fig. 2a. Depending on the experiment, either the second harmonic (532 nm) of a Nd:YAG laser (Continuum Powerlite Precision II 8000) was used to directly excite the gas mixture, or the frequency-doubled output (215–530 nm) of a 355 nm pumped OPO (Continuum Panther) was used for the excitation. The repetition rate of the pulsed laser was 10 Hz and the pulse width was about 10 ns FWHM (Full Width Half Maximum). Without seeding, the line width of the fundamental wavelength is about 1 cm^{-1}. About 100 mJ/pulse of laser energy (532 nm)

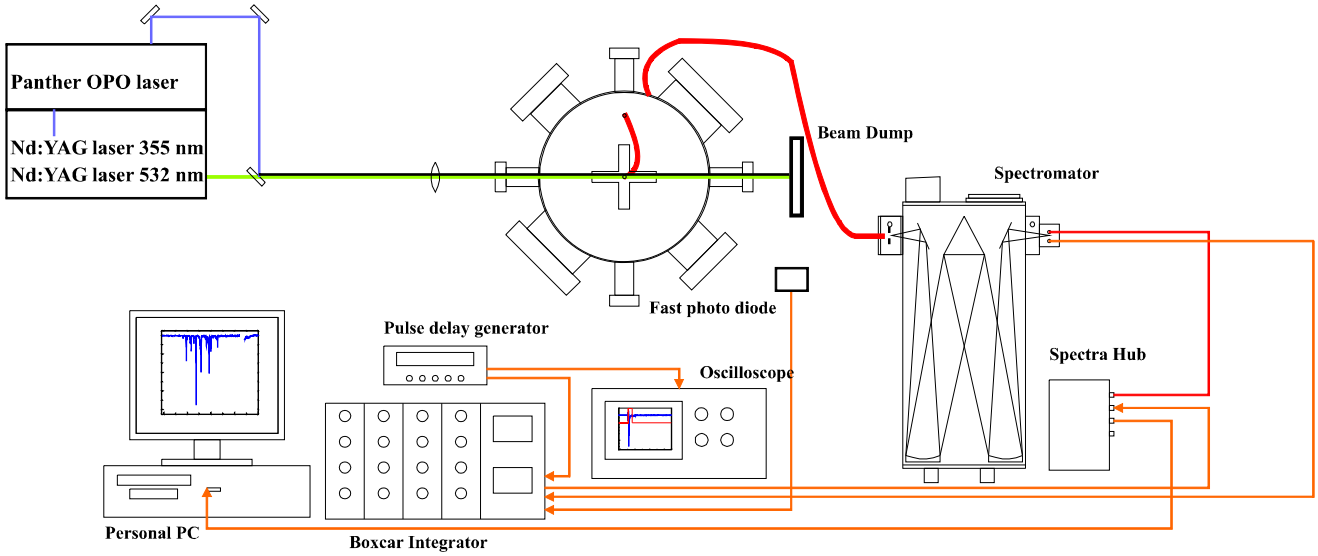

(a)

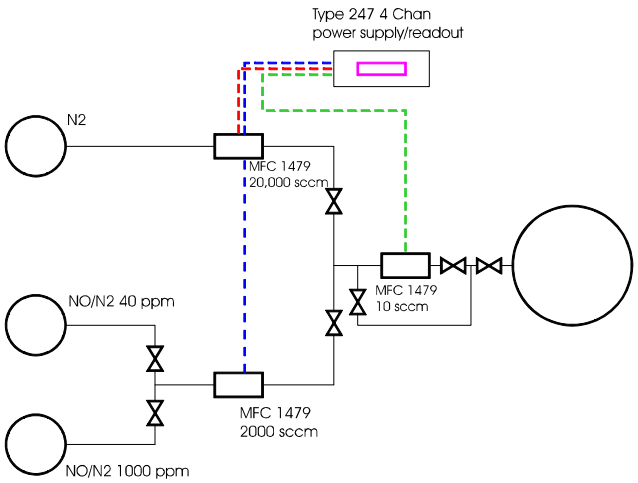

(b)

Fig. 2 (**a**) Schematic of the experimental setup of LIF experiment. (**b**) Schematic of the gas mixing setup

was focused by a 400 mm plano-convex lens (N-BK7, Thorlabs LA1172) into the center of a custom-designed spherical chamber (MDC Vacuum Products LLC), resulting in a power density of about 250 GW/cm^2. The laser energy for 236 nm excitation was about 1 mJ and was focused with a 300 mm lens. The chamber was initially baked out at a temperature of 150°C and then evacuated with a turbo pump (Varian Turbo-V 301 Navigator, 200–280 liters/sec gas dependent), which is backed by a dry scroll vacuum pump (Varian TriScroll 300 Series), to about 10^{-9} Torr. The chamber was then flushed several times using dry N_2 with a purity of 99.999% (UHP grade) before the pure nitrogen experiments.

A schematic of the gas mixing system is shown in Fig. 2b. Three mass flow controllers (MKS 1479 MFC) with flow capacities of 10 sccm, 2000 sccm, and 20000 sccm were used to prepare NO/N_2 gas mixtures with various NO concentrations. N_2 was used as the balancing gas. 40 ppm and 1000 ppm NO balanced with N_2 (Certified Standard) were available for mixing. An MKS type 247 four channel power supply/readout unit was used to control and read the flow rate during mixing.

The fluorescence is collected using a metal coated silica fiber bundle (JT Ingram Technologies Inc, FO10UV-275, 1000 μm). After passing a fiber-optic throughput, an Acton fiber bundle (1rARC-LG-455-020-1) which is rectangularly shaped at the exit end to match the entrance slit of the monochromator (Acton Research Corporation, SpectraPro-2500i, f/6.5), is used to collect the fluorescence.

A cross-shaped optical baffle is mounted at the center of the vacuum cell. The collecting end of the fiber bundle is mounted perpendicularly to the laser beam underneath the

optical baffle. The fluorescence light is collected by a photomultiplier (Hamamatsu R955). The monochromator disperses the fluorescence light via an 1800 g/mm holographic grating (68 × 68 mm). The entrance slit width and exit slit width were set to 300 µm. The spectral resolution for this setup was calculated to be 0.3 nm.

The fluorescence signal from the photomultiplier was observed by an Oscilloscope (Tektronix TDS 3052B) and sent to a boxcar integrator (SRS SR250) where a gate can be set to integrate the transient fluorescence signal. An active baseline subtraction technique was used. The laser was triggered by a digital delay generator (SRS DG645) with 10 Hz frequency whereas the boxcar was triggered at twice the laser frequency. The background was inverted at every other trigger with no signal present and added to the average output of the gated integrator, significantly reducing any baseline drift. The pulse-to-pulse fluctuation of the laser was normalized with an SR235 analog processor. The averaged output of the signal and the laser power from a fast photodiode (Electro-Optics Technology, Inc., Silicon PIN detector ET-2000) were ratioed in the analog processor, and the ratio of signal intensity and laser energy was sent to a Spectra-Hub detector interface (Acton Research Corporation) via the output of the analog processor. The signals were averaged for 3 s in the boxcar. In case of low SN ratios, 10 spectra were averaged.

The voltage output from the analog processor through the Spectra-Hub was sent to a personal computer for data recording. SpectraSense (Princeton Instruments) V 5.0.0 was used to adjust monochromator parameters such as PMT voltage and scanning speed. The signal intensity as a function of wavelength was also recorded by SpectraSense and stored as an ASCII file. Recorded ASCII data were processed with Origin 8.0 software.

3 Results and discussion

This section is divided into three parts. In Sect. 3.1 we demonstrate that molecular nitrogen can be excited by 532 nm through a multi-photon process, resulting in the observation of the N_2 second positive system (2nd PS)—$C^3\Pi_u$–$B^3\Pi_g$—and the N_2^+ first negative system (1st NS)—$B^2\Sigma_u^+$–$X^2\Sigma_g^+$. In Sect. 3.2 we demonstrate energy transfer from laser-excited (532 nm) N_2 to NO, by exciting N_2 and observing the NO γ-band. In Sect. 3.3 we observe emission of the NO γ-band after laser excitation (236 nm) of an NO/N_2 mixture. This emission can be explained with energy transfer from laser-excited nitrogen. Laser excitation with 247 nm did not result in any significant γ-band emission, indicating that excitation of the $X^2\Pi$ $(v''=2) \rightarrow A^2\Sigma$ $(v'=0)$ transition and fluorescence from the $A^2\Sigma$ $(v'=0) \rightarrow X^2\Pi$ $(v''=0)$ transition is the most promising implementation for the detection of explosive materials using the discussed approach.

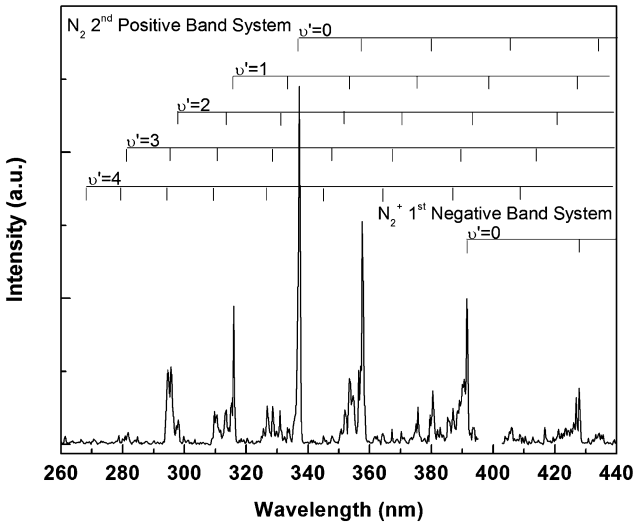

(a)

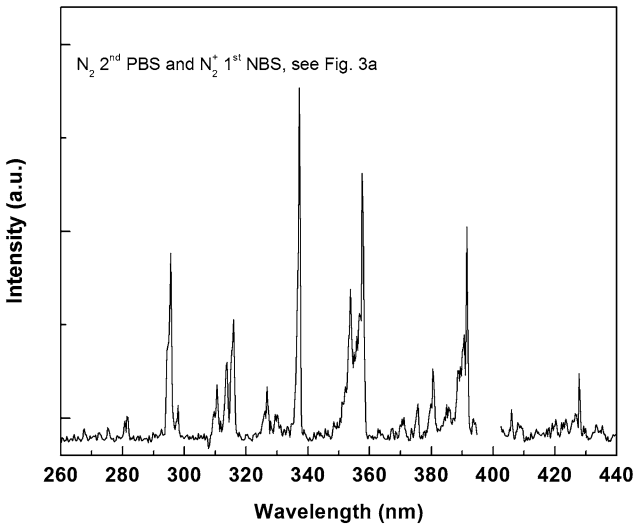

(b)

Fig. 3 (**a**) LIF spectrum of N_2 and N_2^+ in nitrogen excited/ionized by 532 nm. (**b**) LIF spectrum of N_2 and N_2^+ in dry air excited/ionized by 532 nm

3.1 Excitation of N_2 via 532 nm

While laser excitation of molecular nitrogen has been reported for 355 nm (third harmonic of Nd:YAG laser) and 266 nm (forth harmonic of Nd:YAG laser), we demonstrate here the laser excitation of molecular nitrogen using 532 nm (second harmonic of Nd:YAG laser). The emission spectrum resulting from the multi-photon excitation/ionization at 532 nm of the N_2 and N_2^+ in nitrogen is shown in Fig. 3a. The fluorescence spectrum is dominated by the N_2 second positive band system ($C^3\Pi_u$–$B^3\Pi_g$). Two additional major transitions, corresponding to $\Delta v = 0.1$ of the N_2^+ first negative

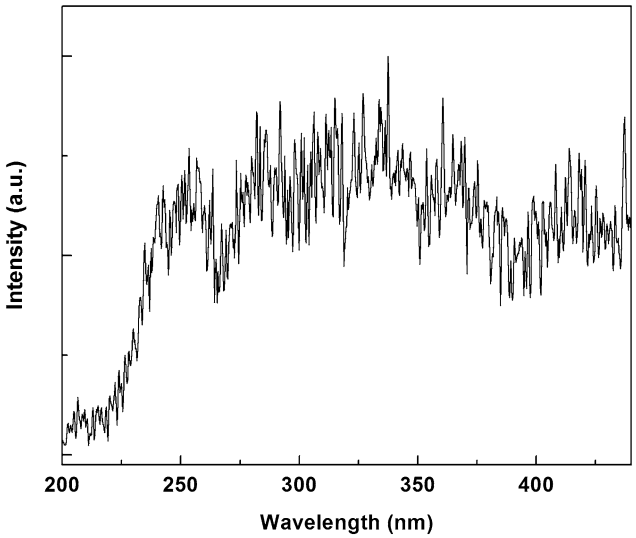

Fig. 4 Breakdown spectrum of nitrogen for excitation with 532 nm

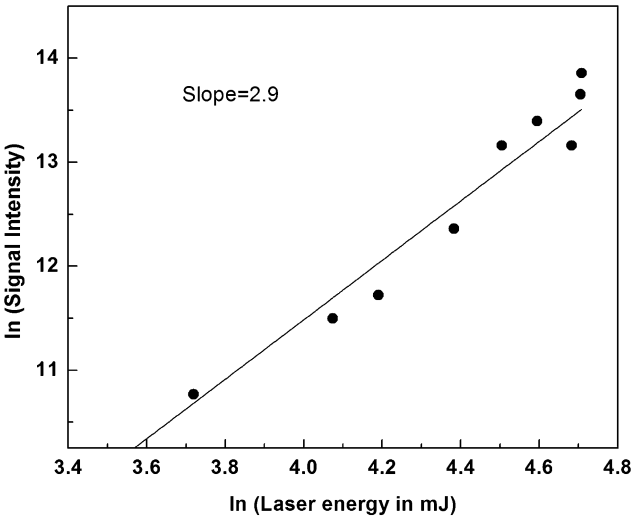

Fig. 6 Log-log plot of signal strength vs. laser energy

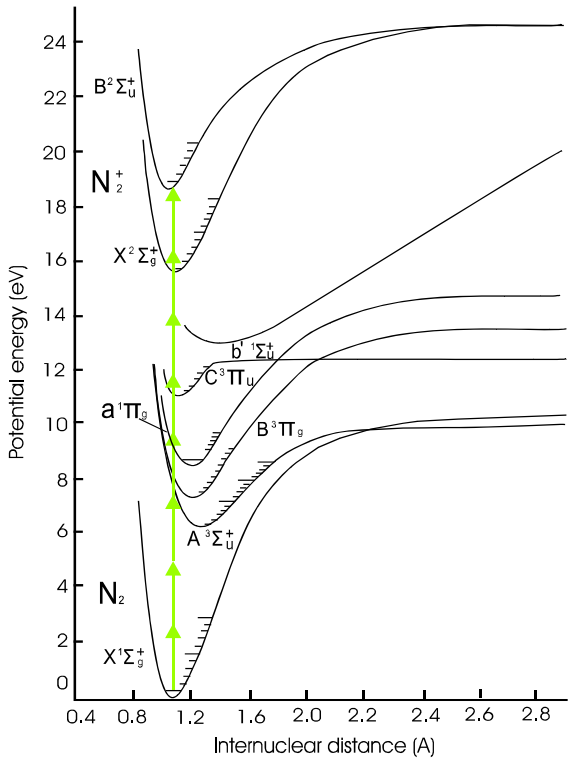

Fig. 5 Potential energy curves for N_2 and N_2^+ and potential multi-photon excitation/ ionization mechanism for 532 nm photons in N_2

band system ($B^2\Sigma_u^+$–$X^2\Sigma_g^+$), are also present. The spectrum also contains some unknown broad-structured emission band between 395 nm and 403 nm. This emission is possibly due to fluorescence from the windows in the vacuum chamber—it also appears under vacuum conditions, without any gas present, and therefore has been omitted in Fig. 3a.

Figure 3b shows the 532 nm excited LIF spectrum of dry air. Again, the N_2 second positive band system ($C^3\Pi_u$–$B^3\Pi_g$) and the N_2^+ first negative band system ($B^2\Sigma_u^+$–$X^2\Sigma_g^+$) are clearly present. The intensities of the spectral lines in Fig. 3b are significantly smaller than those shown in Fig. 3a, indicating the quenching effect of O_2. For reference purposes we also measured the emission spectrum for breakdown in N_2 for high laser intensities with tighter focusing conditions, see Fig. 4. As expected, the breakdown spectrum (plasma) is very broad compared to the molecular spectra shown in Figs. 3a and 3b. Laufer et al. claim that six photons of 355 nm are required for the ionization of the neutral species to the ionic $B^2\Sigma_u^+$ state with $\nu' = 8$ [26]. Their spectrum shows possible emission transitions from up to $\nu' = 5$. In our case, only emission from the $\nu' = 0$ state is apparent. Our spectrum is similar to the one shown by Lewis et al. [27] in the sense that both the second positive system and the first negative system were observed in their spectrum as well as ours. However, the second positive system in our spectrum shows more than just the two major transitions observed at 337.1 nm (0, 0) and 357.6 nm (0, 1) in their work. Vibrational states up to $\nu' = 4$ were populated in our case, possibly due to a slightly different excitation mechanism.

Based on literature data, the potential energy curves of N_2 and N_2^+ are plotted in Fig. 5 [33]. Nee et al. recorded the absorption spectrum of the Tanaka system by exciting N_2 molecules using vacuum ultra violet (VUV) synchrotron radiation [34]. According to their data, the $C^3\Pi_u$ $\nu' = 2$ and $\nu' = 3$ states are located at 92936.8 cm^{-1} and 94696.97 cm^{-1}, respectively.

Lewis et al. claim that two-photon excitation at 266 nm first excites N_2 molecules to the electronically excited $a^1\Pi_g$ state (LBH system), which is followed by the absorption of one more photon to reach the $b'^1\Sigma_g^+$ state [27]. Subsequent

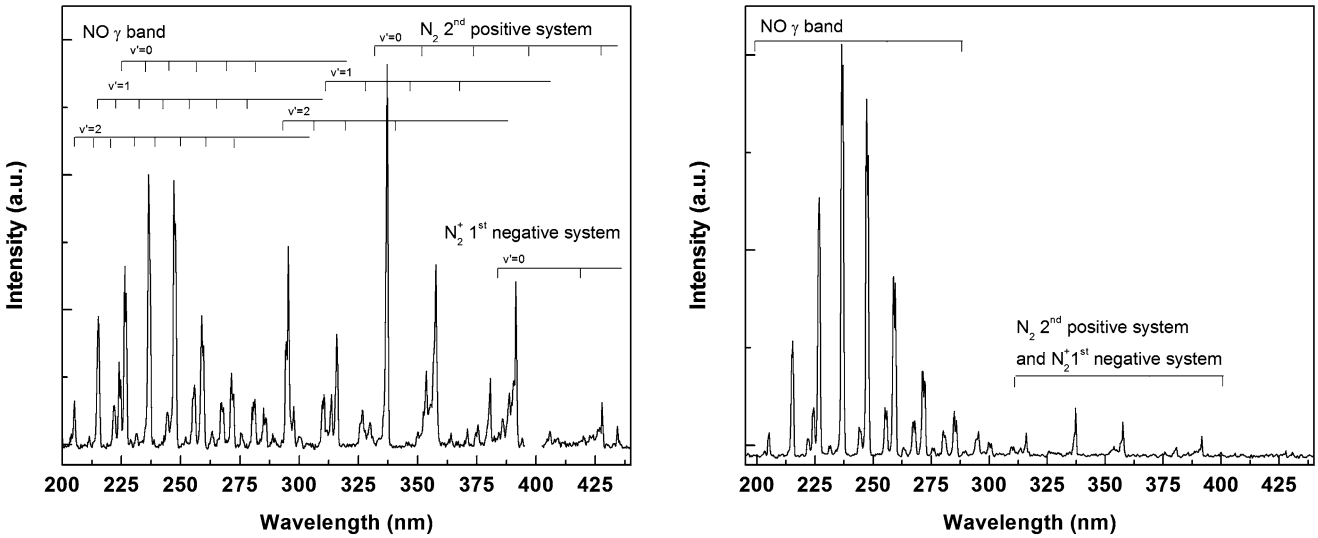

Fig. 7 LIF from 1000 ppm NO in N_2. The spectrum on the left was taken with a short gate and the one on the right with a long gate. The NO γ-band has a significantly longer fluorescence lifetime than the emission from N_2 and N_2^+

quenching from $b'^1\Sigma_g^+$ state to $C^3\Pi_u$ results in the emission of the second positive band system.

Our excitation mechanism is somewhat different—three 532 nm photons have enough energy to reach the $N_2(A^3\Sigma_u^+)$ state, possibly $v' = 5$ [26]. Laser intensity dependent measurements confirm that the limiting step is of third order, see Fig. 6. The data were taken varying the laser power while monitoring the signal strength of the emission at 337.1 nm ($C^3\Pi_u$–$B^3\Pi_g$ 0–0). The Frank–Condon factor for the absorption from the ground state to v' (5) is among the largest [26]. The N_2 $A^3\Sigma_u^+ \leftarrow X^1\Sigma_g^+$ transition (Vegard–Kaplan system) violates the spin selection rule and the transition probability is small. Nevertheless, the Vegard–Kaplan system has been observed in absorption, although only for $v' \geq 6$ due to the small Frank–Condon factors for transitions to lower vibrational levels [35, 36]. Energetically, by absorbing one more photon, the $a^1\Pi_g$ state can be reached. Finally, absorbing a fifth photon could result in the excitation of the $C^3\Pi_u$ state. The energy of five photons from the second harmonic of a Nd:YAG laser (532.075 nm) is 93971 cm^{-1}. The energy of the $C^3\Pi_u$ $v' = 3$ state (94696.97 cm^{-1}) is 726 cm^{-1} higher than the energy of five 532.075 nm photons. Taking the room temperature energy ($kT \sim 200$ cm^{-1}) into account, there is an energy deficit of about 526 cm^{-1}. According to Lewis et al., laser heating would be able to account for this difference [27]. In that case, five laser photons would result in the excitation of the $C^3\Pi_u$ $v' = 3$ state and the subsequent $C^3\Pi_u \rightarrow B^3\Pi_g$ fluorescence.

Absorbing three more photons leads to the photo-ionization of molecular nitrogen. The energy of eight 532.075 nm photons is about 150354.7 cm^{-1}. 151233.5 cm^{-1} is needed to excite the $B^2\Sigma_u^+$ state of N_2^+ from the ground state of N_2 [37]. Similar to the N_2 ($C^3\Pi_u$) state excitation case, laser heating should be enough to match the energy deficit. The observation of the first negative system indicates this excitation. The emission observed at 391.4 nm (0, 0) and 427.7 nm (0, 1) indicates that only low vibrational states in $B^2\Sigma_u^+$ are populated. While the absorption of four additional photons cannot be completely ruled out, there is no indication of fluorescence from higher-lying vibrational states. As such, the absorption of three additional photons combined with laser heating appears more likely.

Comparing the two nitrogen spectra taken in N_2 and in dry air, the quenching of the fluorescence intensity for both the second positive system and the first negative system was apparent in the dry air sample. The presence of O_2 is believed to be responsible for the quenching. For example, the charge-exchange reaction $N_2^+ + O_2 \rightarrow O_2^+ + N_2$, is well known [27]. Pancheshnyi et al. measured the rate constant of N_2 ($C^3\Pi_u$, $v' = 0$) and N_2^+ ($B^2\Sigma_u^+$, $v' = 0$) deactivation by O_2 and obtained deactivation rate constants of $2.7 \pm 0.3 \times 10^{-10}$ cm^3/s for N_2 ($C^3\Pi_u$, $v' = 0$) and $5.1 \pm 0.5 \times 10^{-10}$ cm^3/s for N_2^+ ($B^2\Sigma_u^+$, $v' = 0$) [38]. It is apparent that among other quenching mechanisms, the presence of O_2 plays a very important role.

3.2 Energy transfer from laser-excited (532 nm) nitrogen to NO

The emission spectra of a mixture of 1000 ppm NO in N_2 at atmospheric pressure for excitation with 532 nm are shown in Fig. 7. The spectra show the NO γ-band, the second positive system of N_2, and the first negative system of N_2^+. To obtain the spectra, the gate was set immediately following the laser pulse. The integration time was set to about 120 ns (left spectrum) and 3 µs (right spectrum). Comparison of

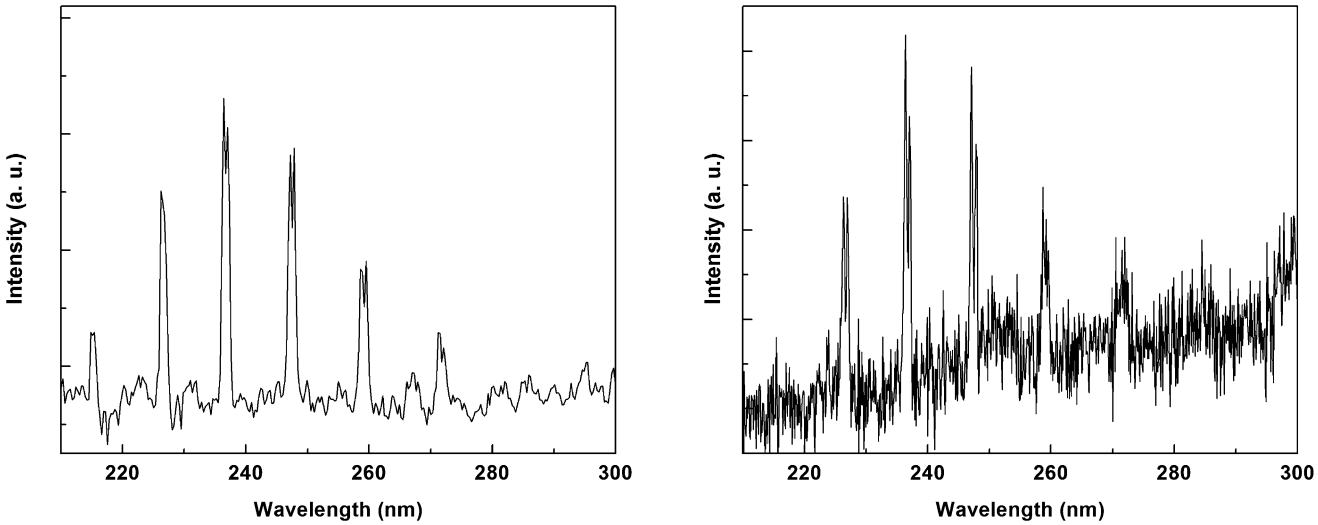

Fig. 8 LIF from 40 ppm (*left*) and 200 ppb (*right*) NO in N_2

the two spectra indicates that the fluorescence lifetime of the NO γ-band emission is significantly longer than the fluorescence lifetime of the fast decaying N_2 and N_2^+ transitions.

The NO γ-band dominates the transitions between 200 nm and 300 nm, except for the N_2 $C^3\Pi_u \rightarrow B^3\Pi_g$ $(4, 2)$ transition at 295.3 nm. Most of the NO transitions show double peak structures, demonstrating the splitting of the NO ground state into $X^2\Pi_{1/2}$ and $X^2\Pi_{3/2}$ levels. The major transitions between 300 nm and 400 nm correspond to the N_2 second positive band system ($C^3\Pi_u \rightarrow B^3\Pi_g$). The transitions at 391.4 nm $(0, 0)$, and 427.7 nm $(0, 1)$ belong to the first negative system of N_2^+ ($B^2\Sigma_u^+ \rightarrow X^2\Sigma_g^+$). Using a short gate, a broad-structured emission between 395 nm and 403 nm was observed. This emission, which was also observed under vacuum, is possibly due to fluorescence from the vacuum chamber windows. With a longer gate width, this fast decaying component was not observed in the right panel of Fig. 7. For comparison reasons, it has been omitted from the spectrum in the left panel of Fig. 7.

To demonstrate the sensitivity of the energy transfer process by measuring the NO γ-band, we performed some measurement with lower concentration of NO in N_2. Figure 8 shows the NO spectra due to energy transfer from laser-excited N_2 for NO concentrations of 40 ppm (left) and 200 ppb (right), respectively. The 200 ppb concentration was estimated based upon mixing 40 ppm NO/N_2 with pure N_2. Because of the very long lifetime of the emission in 200 ppb NO, this spectra was taken in cw mode, without the boxcar integrator. In this case the signal was averaged 100 times. Even lower concentrations are expected to be observable by using a lens system to focus the emitted light into the collecting fiber. Such a lens system is expected to increase the collection efficiency by a factor of about 150.

Figure 9 shows the energy levels of N_2 and NO. N_2 is excited by 532 nm via a multi-photon excitation process. The fact that the second positive system of N_2, and the first negative system of N_2^+ are observed, indicates that $N_2(C^3\Pi_u)$ and $N_2^+(B^2\Sigma_u^+)$ are populated during the excitation. Subsequently, N_2 relaxes into the $A^3\Sigma_u^+$, which is a long-lived metastable state. During collisions with NO, energy can be transferred from $N_2(A^3\Sigma_u^+)$ to $NO(A^2\Sigma^+)$, as indicated by the red arrow in Fig. 9.

The excited NO molecules can then relax to their electronic ground state under emission of light (γ-band). In this case, the observed fluorescence lifetime is determined by the energy-transfer process. Settersten et al. measured the decay rates of NO ($A^2\Sigma^+$, $\nu' = 0, 1, 2$). By extrapolating to zero pressure, they obtained radiative lifetimes of 192.6 ± 0.2 ns for $\nu' = 0$, 186.2 ± 0.4 ns for $\nu' = 1$, and 179.4 ± 0.7 ns for $\nu' = 2$ [39]. As mentioned before, in their energy transfer experiment, Young et al. observed a decay time of the NO γ-band which was much longer than the natural radiative lifetime, and concluded it was due to the collisional energy transfer from $N_2(A^3\Sigma_u^+)$ to $NO(X^2\Pi_r)$ [40]. Similarly, Luque et al. measured NO $A \rightarrow X\,(0, 1)$, $(4, 6)$, and $(3, 5)$ bands at 236 nm after excitation of the NO $(A, \nu' = 4)$ band in a gas mixture of 0.4 Torr of NO and 100 Torr of nitrogen [41]. It showed multi-exponential behavior of the time-decays of 8 ns, 0.136 µs, and 1.2 µs. They concluded that the observations strongly suggested a resonant energy transfer mechanism.

Figure 10 shows the fluorescence lifetime of 1000 ppm NO in N_2 after excitation with 532 nm at atmospheric pressure. The emission was observed at 236 nm, corresponding to the $A^2\Sigma^+$ $(\upsilon' = 0)$ to $X^2\Pi$ $(\upsilon'' = 1)$ transition. The data can be fitted with a single exponential decay with a time constant of 0.95 µs. This time constant is significantly longer

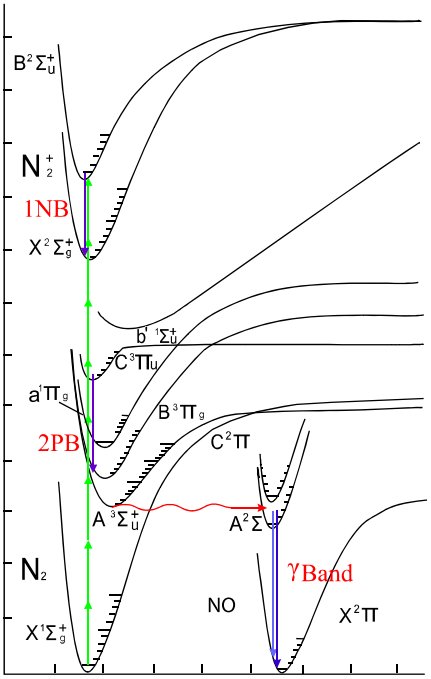

Fig. 9 Energy levels of N_2 and NO, and the respective excitation, fluorescence, and energy transfer pathways

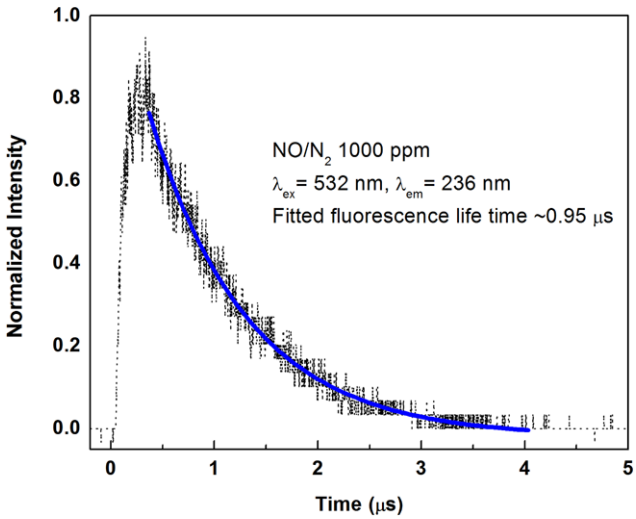

Fig. 10 Fluorescence lifetime of 1000 ppm NO in N_2 for 532 nm excitation and 236 nm observation

than the time constant of about 200 ns for direct excitation and confirms the presence of the energy transfer mechanism. The decay constants for lower concentrations of NO were even longer. However, because of the weak signals, no direct measurement of the decay constants was possible.

The quenching of the $N_2(A^3\Sigma_u^+)$ state by NO molecules is thought to happen by a nearly resonant energy transfer mechanism:

$$N_2(A^3\Sigma_u^+) + NO(X^2\Pi_r) \xrightarrow{k_1} N_2(X^1\Sigma_g^+) + NO(A^2\Sigma^+). \tag{1}$$

$$NO(A^2\Sigma^+) \xrightarrow{k_2} NO(X^2\Pi_r) + h\nu. \tag{2}$$

In (1), k_1 is the rate constant of the reaction, and in (2) $k_2 = 1/\tau_0$, where $\tau_0 \approx 200$ ns is the radiative lifetime of $NO(A^2\Sigma^+)$. The described mechanism excludes reactions which are slower than collisions, such as the radiative decay of $N_2(A^3\Sigma_u^+)$. We also did not consider the collision between $NO^*(A^2\Sigma^+)$ and $NO(X^2\Pi)$. In addition, we assume that at time zero, no detectable amount of $NO(A^2\Sigma^+)$ is formed directly by laser excitation. Using an approach similar to that of Le Calve et al. [42], we find that the resolution of this simple system leads to

$$[NO^*] = [NO^*]_0 e^{-k_2 t} + \frac{k_1[N_2^*]_0}{k_2 - k_1}\left(e^{-k_1 t} - e^{-k_2 t}\right). \tag{3}$$

At time zero, $[NO^*]_0 = 0$. Therefore, (3) simplifies to

$$[NO^*] = \frac{k_1[N_2^*]_0}{k_2 - k_1}\left(e^{-k_1 t} - e^{-k_2 t}\right), \tag{4}$$

where $[NO^*]$ is the $NO(A^2\Sigma^+)$ concentration, and $[NO^*]_0$ and $[N_2^*]_0$ are the initial concentrations of $NO(A^2\Sigma^+)$ and $N_2(A^3\Sigma_u^+)$, respectively. Since the decay constant τ obtained by the fitting procedure is greater than the radiative lifetime of $NO(A^2\Sigma^+)$ τ_0, the first exponential term in (4) governs the signal decay kinetics.

3.3 Energy transfer from laser-excited (236 nm) nitrogen to NO

The emission spectra of a mixture of 1000 ppmV NO in N_2 and 1 ppmV NO in N_2 for excitation with 236 nm are shown in Fig. 11. The peak at 236 nm is partially due to the laser excitation wavelength. Both spectra clearly show the NO γ-band. Even though the NO concentration of the sample in the right panel of Fig. 11 is three orders of magnitude lower than the sample in the left panel, the signal is still very strong and the SN ratios are similar. This strong signal for the 1 ppmV NO/N_2 sample suggests that significantly lower concentration can also be detected and make the energy transfer issue relevant for explosion detection with ambient NO levels of about 1 ppbV.

According to the Boltzmann statistics, the relative population of NO ($v'' = 1$) is about 10^{-5} at room temperature compared to the NO ($v'' = 0$) [24]. As such, it appears highly unlikely that such strong γ-bands would be observed for direct excitation of the NO $X^2\Pi$ ($v'' = 1$) $\rightarrow$ $A^2\Sigma$ ($v' = 0$) transition. The observed fluorescence lifetime for excitation with 236 nm and observation at 226 nm yielded a single

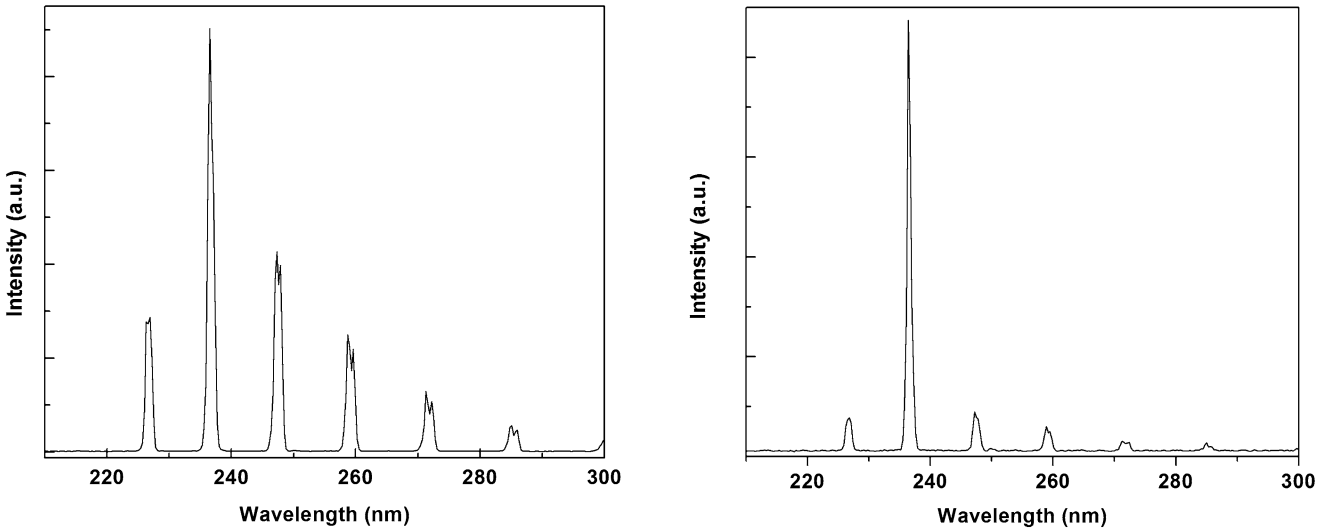

Fig. 11 Emission spectra of 1000 ppm NO in N_2 (*left*) and 1 ppm NO in N_2 (*right*) for excitation at 236 nm

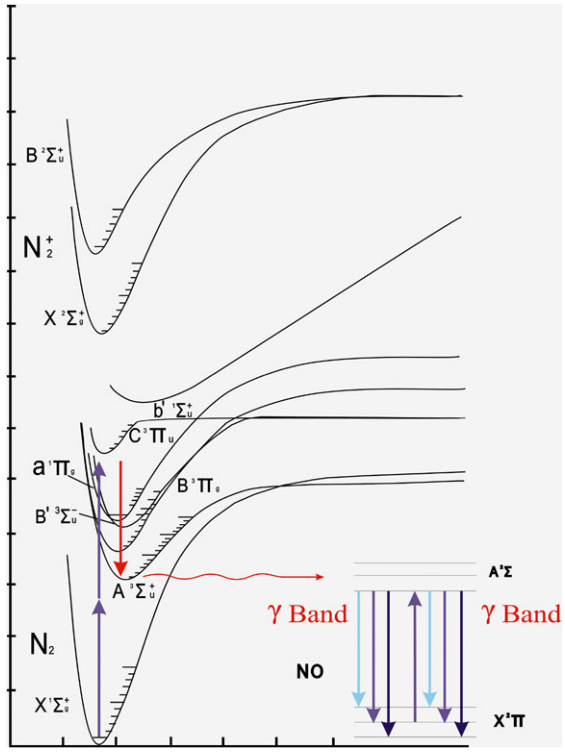

Fig. 12 Energy transfer from laser-excited nitrogen followed by NO emission

exponential decay with a value of 88 ns at atmospheric pressure. Reference spectra of pure N_2 and dry air using 236 nm for the excitation show that no NO γ-bands are observed under these conditions. However, a review of the optical absorption spectra of molecular nitrogen shows that molecular nitrogen has a resonance absorption at 118.1499 nm, corresponding to the N_2 $X^1\Sigma_g^+$ $(\nu'' = 0) \rightarrow B'^3\Sigma_u^-$ $(\nu' = 14)$ transition [33]. As such, a two-photon absorption process of 236 nm could take place to excite molecular nitrogen, which could lead to energy transfer similar to what we observed for excitation with 532 nm.

Figure 12 shows the N_2 energy levels, including the two-photon absorption of 236 nm and subsequent relaxation, which would again populate the long-lived N_2 $A^3\Sigma_u^+$. During collisions with NO, energy can be transferred from $N_2(A^3\Sigma_u^+)$ to $NO(A^2\Sigma^+)$, with subsequent relaxation and emission of the γ-band. The γ-band emission will populate the various vibrational states of the $NO(X^2\Pi)$ ground state, including the $\nu'' = 1$ state. As soon as this level is populated, 236 nm photons will be absorbed again by NO ($X^2\Pi$, $\nu'' = 1$) and re-excite the molecules back to the $A^2\Sigma^+$ state resulting in further γ-band emission with the characteristic fluorescence lifetime.

A less likely scenario appears to be multiphoton (236 nm) ionization and subsequent recombination of NO^+ capturing a free electron. As Hellberg et al. pointed out, NO^+ ions in their ground state $X^1\Sigma^+$ and first excited state $a^3\Sigma^+$ capture electrons of various collisional energy in the dissociative recombination (DR) process and will generate N and O in various states rather than NO [43]. While determining the exact origin will require further investigations, the main concern here is the observation of the NO γ-band after excitation with 236 nm without a source for vibrationally hot NO present.

As outlined in the introduction, Shu et al. and Arusi-Parpar et al. explored using excitation from the $\nu'' = 2$ level to detect vibrationally hot NO [19–21, 25]. Using our NO/N_2 mixture, we performed an excitation scan to determine interference mechanisms at wavelengths other that 236 nm. The results, shown in Fig. 13, indicate that the observed interference mechanism only acts at about

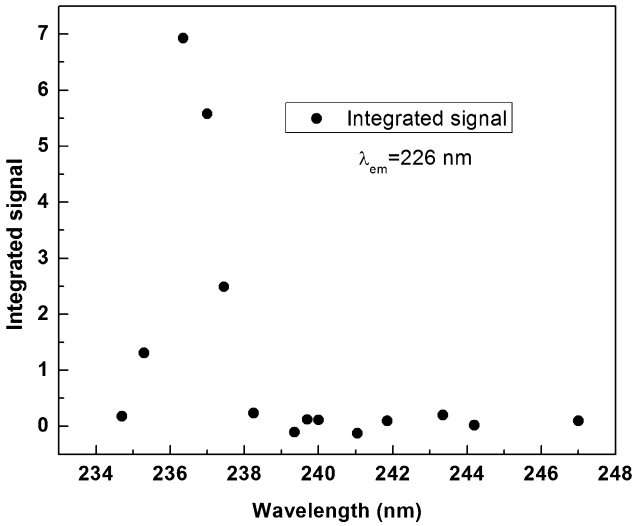

Fig. 13 Excitation spectrum of NO/N_2 showing that excitation occurs only at 236/237 nm

236/237 nm, and is thus limited to excitation from the $\nu'' = 1$ level.

4 Conclusions

Vaporization, photo-fragmentation, and subsequent laser-induced fluorescence is one of the most promising approaches for the detection of explosives, via detection of NO. However, the use of 532 nm and 236 nm laser wavelengths for the detection of nitro-based explosive materials via monitoring vibrationally hot NO is potentially subject to interference from interactions with atmospheric constituents. Exposure to these particular wavelengths leads to the observation of the NO γ-band, even though no vibrationally hot NO is present. This observation can be explained by energy transfer from laser-excited nitrogen to NO. The use of 247–248 nm to vaporize, photo-dissociate, and excite the NO $X^2\Pi$ $(\nu'' = 2) \rightarrow A^2\Sigma$ $(\nu' = 0)$ transition and observe the $A^2\Sigma$ $(\nu' = 0) \rightarrow X^2\Pi$ $(\nu'' = 0)$ fluorescence is not subject to the described interference mechanism, and appears to be a better implementation of this particular detection process.

Acknowledgement This work was supported by ONR grants N00014-10-1-0284 and N00014-04-1-0688.

References

1. D.S. Moore, Rev. Sci. Instrum. **75**, 2499 (2004)
2. S. Singh, J. Hazard. Mater. **144**, 15 (2007)
3. J.I. Steinfeld, J. Wormhoudt, Annu. Rev. Phys. Chem. **49**, 203 (1998)
4. D.O. Henderson, R. Mu, Y.S. Tung, G.C. Huston, Appl. Spectrosc. **49**, 444 (1995)
5. J. Janni, B.D. Gilbert, R.W. Field, J.I. Steinfeld, Spectrochim. Acta, Part A, Mol. Biomol. Spectrosc. **53**, 1375 (1997)
6. N.F. Fell, J.M. Widder, S.V. Medlin, J.B. Morris, R.A. PesceRodriguez, K.L. McNesby, J. Raman Spectrosc. **27**, 97 (1996)
7. K.L. McNesby, C.S. Coffey, J. Phys. Chem. B **101**, 3097 (1997)
8. K.L. Mcnesby, J.E. Wolfe, J.B. Morris, R.A. Pescerodriguez, J. Raman Spectrosc. **25**, 75 (1994)
9. M. Gaft, L. Nagi, Opt. Mater. **30**, 1739 (2008)
10. A. Portnov, I. Bar, S. Rosenwaks, Appl. Phys. B, Lasers Opt. **98**, 529 (2010)
11. D.D. Wu, J.P. Singh, F.Y. Yueh, D.L. Monts, Appl. Opt. **35**, 3998 (1996)
12. H. Zuckermann, G.D. Greenblatt, Y. Haas, J. Phys. Chem. **91**, 5159 (1987)
13. A. Mukherjee, S. Von der Porten, C.K.N. Patel, Appl. Opt. **49**, 2072 (2010)
14. B. Arnold, L. Kelly, J.B. Oleske, A. Schill, Anal. Bioanal. Chem. **395**, 349 (2009)
15. J.L. Gottfried, F.C. De Lucia, C.A. Munson, C. Ford, A.W. Miziolek, Detection of energetic materials and explosive residues with laser-induced breakdown spectroscopy: II. Stand-off measurements, in *Army Research Laboratory* (2007)
16. J.L. Gottfried, F.C. De Lucia, C.A. Munson, A.W. Miziolek, Anal. Bioanal. Chem. **395**, 283 (2009)
17. Y.Q. Guo, A. Bhattacharya, E.R. Bernstein, J. Phys. Chem. A **113**, 85 (2009)
18. C. Mullen, M.J. Coggiola, H. Oser, J. Am. Soc. Mass Spectrom. **20**, 419 (2009)
19. J. Shu, I. Bar, S. Rosenwaks, Appl. Opt. **38**, 4705 (1999)
20. J. Shu, I. Bar, S. Rosenwaks, Appl. Phys. B, Lasers Opt. **71**, 665 (2000)
21. J. Shu, I. Bar, S. Rosenwaks, Appl. Phys. B, Lasers Opt. **70**, 621 (2000)
22. J.D. White, F.A. Akin, H. Oser, D.R. Crosley, Appl. Opt. **50**, 74 (2011)
23. C.M. Wynn, S. Palmacci, R.R. Kunz, K. Clow, M. Rothschild, Appl. Opt. **47**, 5767 (2008)
24. C.M. Wynn, S. Palmacci, R.R. Kunz, M. Rothschild, Opt. Express **18**, 5399 (2010)
25. T. Arusi-Parpar, D. Heflinger, R. Lavi, Appl. Opt. **40**, 6677 (2001)
26. G. Laufer, R.H. Krauss, J.H. Grinstead, Opt. Lett. **16**, 1037 (1991)
27. W.B. Lewis, W.R. Wadt, Chem. Phys. Lett. **78**, 266 (1981)
28. W.G. Clark, D.W. Setser, J. Phys. Chem. **84**, 2225 (1980)
29. C.H. Dugan, J. Chem. Phys. **45**, 87 (1966)
30. T. Hikida, Y. Mori, J. Chem. Phys. **69**, 346 (1978)
31. L.G. Piper, L.M. Cowles, W.T. Rawlins, J. Chem. Phys. **85**, 3369 (1986)
32. J.M. Thomas, D.H. Katayama, Chem. Phys. Lett. **214**, 250 (1993)
33. A. Lofthus, P.H. Krupenie, J. Phys. Chem. Ref. Data **6**, 113 (1977)
34. J.B. Nee, C.Y. Yuan, J. Hsu, W.J. Chen, J.C. Yang, Chem. Phys. **315**, 81 (2005)
35. D.E. Shemansky, J. Chem. Phys. **51**, 689 (1969)
36. P.G. Wilkinson, J. Chem. Phys. **30**, 773 (1959)
37. G. Dilecce, P.F. Ambrico, S. De Benedictis, Plasma Sources Sci. Technol. **14**, 561 (2005)
38. S.V. Pancheshnyi, S.M. Starikovskaia, A.Y. Starikovskii, Chem. Phys. Lett. **294**, 523 (1998)
39. T.B. Settersten, B.D. Patterson, W.H. Humphries, J. Chem. Phys. **131**, (2009)
40. R.A. Young, G.A.St. John, J. Chem. Phys. **48**, 898 (1968)
41. J. Luque, D.R. Crosley, J. Phys. Chem. A **104**, 2567 (2000)
42. J. Le Calve, J. Chem. Phys. **58**, 1446 (1973)
43. F. Hellberg, S. Rosen, R. Thomas, A. Neau, M. Larsson, A. Petrignani, W.J. van der Zande, J. Chem. Phys. **118**, 6250 (2003)